Proc. NIPR Symp. Polar Meteorol. Glaciol., 2, 142-151, 1989

RADIO SCATTERING CHARACTERISTICS OF ANTARCTIC ICE SHEET USING AIRBORNE RADIO ECHO SOUNDING DATA

Seiho URATSUKA[1], Fumihiko NISHIO[2], Hirokazu OHMAE[3] and Shinji MAE[4]

[1]*Communications Research Laboratory, Ministry of Posts and Telecommunications, 2-1, Nukui-kitamachi 4-chome, Koganei 184*
[2]*National Institute of Polar Research, 9-10, Kaga 1-chome, Itabashi-ku, Tokyo 173*
[3]*Institute of Low Temperature Science, Hokkaido University, Kita-19, Nishi-8, Kita-ku, Sapporo 060*
[4]*Department of Applied Physics, Faculty of Engineering, Hokkaido University, Kita-13, Nishi-8, Kita-ku, Sapporo 060*

Abstract: Some characteristics of radio wave scattering from ice sheet surfaces, inner volume and the bedrock surface are inferred from data obtained from 179 MHz airborne radio echo sounder data during the 27th Japanese Antarctic Research Expedition. A-scope data from sounder with wide antenna beams include information on the scattering characteristics at the ice sheet surface, within the ice sheet itself, and at the bedrock sub-surface. Characteristics are modeled from the A-scope form by using expanded radar equations which allow determination of the roughness of the ice sheet and bedrock surfaces.

Results indicate a strong dependence of backscatter from the ice surface with incidence angle and a weak dependence in backscatter from the bedrock.

1. Introduction

The radio echo sounding method has been used to measure the ice sheet thickness by many glaciologists, and many efforts have been made to map the Antarctic ice sheet thickness and bedrock. This method is an application of a pulse radar system. Usually, the frequencies of radio echo sounders are chosen in the VHF band because of its low attenuation characteristics in ice. The pulsed radio waves are transmitted toward the ice sheet surface from an airborne or snow-vehicle-borne antenna, and the ice thickness is calculated by the time difference between return signals from the ice sheet surface and bedrock. The received signals on the A-scope of this sounder system, however, don't have a simple form like two sharp peaks but a more complicated form similar to weather radars, as shown in Fig. 1. Figure 1 shows 7 examples from the A-scope of the airborne radio echo sounder. In each case, data were observed every 10 s about 100 km west of Asuka Camp. These complex figures are composed of surface scattering from ice sheet and bedrock, and volume scattering from the ice interior.

Reflcetions from inner layers in the ice sheet have been discussed by, for example,

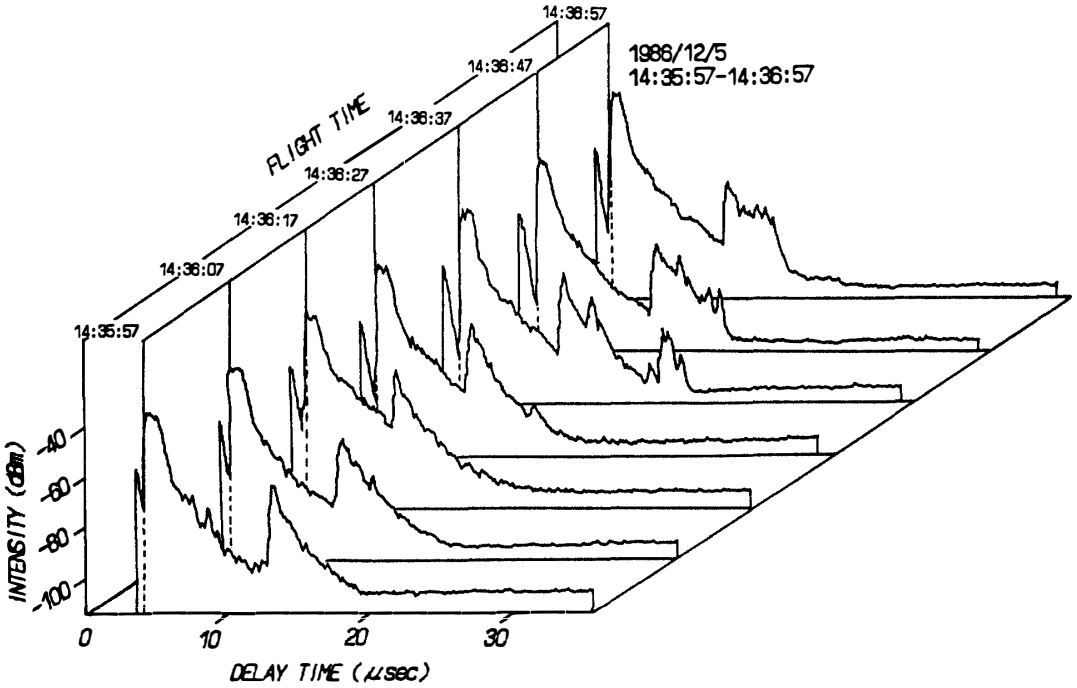

Fig. 1. Examples of A-scopes of airborne radio echo sounder.

HARRISON (1973) and PAREN and ROBIN (1975). They used the concept of reflection coefficient but the physical meaning of reflection coefficients becomes uncertain for the case of a system with a wide antenna beam and a pulse length which is greater than the separation between ice layers. We propose to use a volumetric scattering coefficient for the ice interior, because this parameter gives a more precise and reasonable estimation in the whole volume of the pulse than a reflection coefficient does.

In addition, the scattering coefficient of the ice sheet surface or bedrock surface is analyzed by using the wide antenna beam pattern of the radio echo sounder. The scattering characteristics of ice sheet surface and bedrock surface have been discussed by NEAL (1976). He used the "ESM recording" method, which is a continuous quantitative record of the peak of the returned power, in oder to measure surface roughness, but it seems to be possible to also estimate scattering characteristics of both the ice sheet surface and bedrock from the A-scope pattern of a sounder with a wide beam, as will be explained in section 3.

In this paper, we will try to infer the scattering characteristics of the ice sheet surface, the inner ice sheet volume and the bedrock sub-surface from data obtained during the 27th Japanese Antarctic Research Expedition.

2. Summary of the Airborne Radio Echo Sounder

Radio echo sounding has been conducted in the Japanese Antarctic research program since 1968. The newest radio echo sounder system (NIPR-III) was developed in 1985. The major parameters of the system are shown in Table 1, and a block diagram in Fig. 2. The system is able to detect up to 2800 m ice thickness. This system was installed on a Pilatus PC-6 aircraft, and transmitting and receiving antennas

Table 1. Major characteristics of 179 MHz airborne radio echo sounder system.

Transmitter	Frequency	179 MHz
	Peak power	1 kW
	Pulse width	60/250/1000 ns
	Resolution in air	9/37.5/150 m
	in ice[1]	5.1/21.4/85.5 m
	Repetition period	1 ms
Receiver	Sensitivity[2]	−110 dBm
	Band width	14/4/1 MHz
	Noise figure	<1 dB
Antenna	Type	3 element Yagi
	Gain	8.15 dBi
	Beam width	70 degrees
Recording	Digital	1/4 inch cartridge tape
	(binary)	324 byte every 0.5 s (10 MHz sampling)
	(ASCII)	VLF/Omega, GPS, Barometric and Radio Altimeter, Gyro, and Thermometer
	Analogue	8 mm VTR (back-up)

[1] We assumed that the refractive index is 1.78.
[2] Receiver band width is 4 MHz.

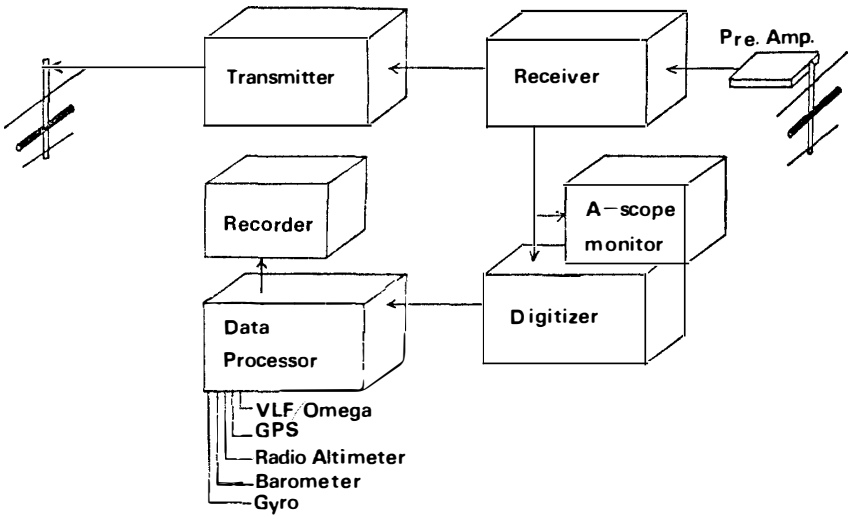

Fig. 2. Block diagram of airborne radio echo sounder system.

were set under the right and left wings of this aircraft, respectively. Because of payload size restrictions, we chose 179 MHz and a 3-element Yagi antenna with wide beam antenna (70 degrees).

The received signals are initially amplified by a low noise preamplifier set under the wing. This amplifier includes a limiter to protect the main receiver system from strong signals. The maximum signal level is −30 dBm and the minimum is −110 dBm, for a total dynamic signal range 80 dB. Output signals are provided to a digitizer and to an A-scope monitor with a timing signal for pulse transmission. In the digitizer,

256 frames of digitized signals are averaged over a period of 0.5 s, where one frame is composed of the returning signal train from one pulse. Two of these average signals from the digitizer are combined to form a 811 byte record every second in the data processor together with navigation data consisting of altitude (radio and barometric altimeter with thermometer), position (VLF/omega and GPS receiver), and attitude (Gyro). Finally, the formatted data are recorded by a 1/4 inch digital cartridge recorder.

3. Radar Equations

Typical received data from the Antarctic ice sheet in A-scope form have the characteristic pattern shown in Fig. 1. These patterns are formed by characteristic curves with fine fluctuations, and can be considered to be the superimposition of three curves

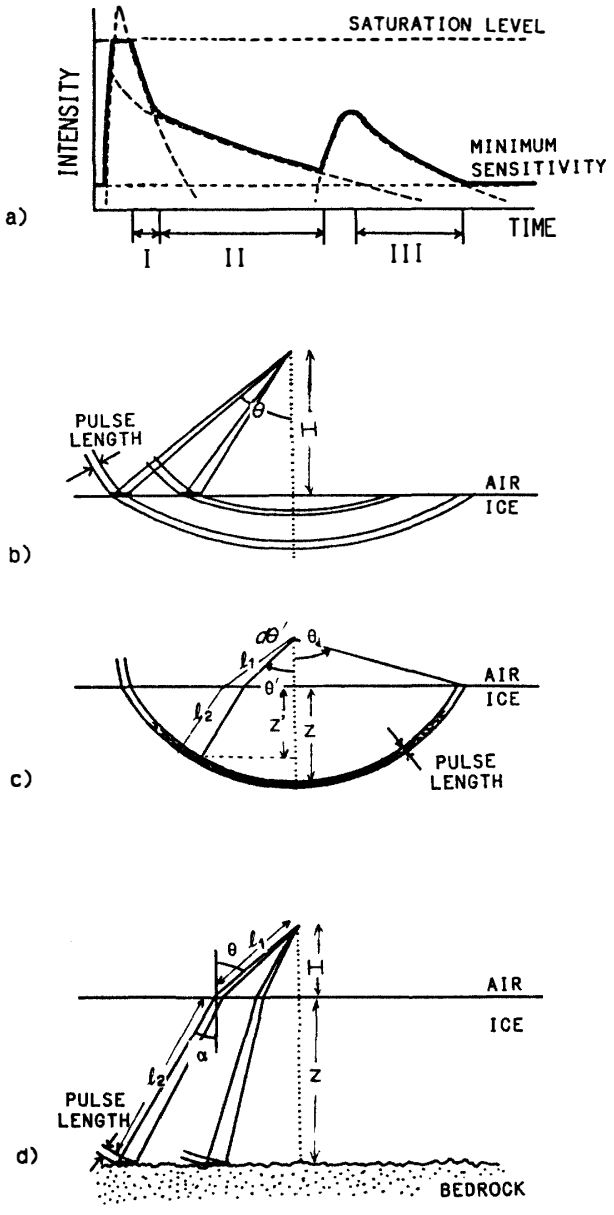

Fig. 3. (a) Schematic pattern of A-scope figure and divided parts. (b) Scattering area at ice surface and incident angle. (c) Scattering volume at inner ice sheet. (d) Scattering area at bottom of ice sheet and incidence angle.

as indicated by dashed curves in Fig. 3(a). The three parts indicated by the dashed curves can be separated by differences in the return time. These three parts are noted by (I), (II), and (III) in Fig. 3(a). Signal parts (I), (II), and (III) correspond to contributions from the ice sheet surface as shown in Fig. 3(b), the inner region of the ice sheet as shown in Fig. 3(c), and bedrock surface as shown in Fig. 3(d), respectively. Therefore, we can derive three radar equations, which represent the effects of an antenna pattern with wide beam, for each part.

This method aims at inferring the unkown parameters of these equations, namely: the backward scattering coefficient of the ice sheet surface and the bedrock surface, the volume scattering coefficient of the ice interior, and attenuation coefficient of ice. The meanings of these parameters are discussed in Section 5 and the radar equations of each region are given in the subsection below.

3.1. Radar equation for ice sheet surface

The round-trip time (delay time) τ of the transmitted pulse depends on the propagation path length related to the incidence angle θ and is expressed as $\tau=2H/(c\cos\theta)$, where H is the aircraft altitude, and c is the speed of light. Moreover, the received power P_r from ice sheet surface is given as follows:

$$P_r=\frac{P_tG^2\lambda^2h\sigma_s^0(\theta)f^2(\theta)\cos^3\theta}{2^6\pi^2H^3L^2} \tag{1}$$

here,

P_t: transmitted power
h: pulse length in free space
λ: wavelength in free space
G: antenna peak gain
$f(\theta)$: antenna pattern (assumed azimuthally symmetric)
L: system loss
$\sigma_s^0(\theta)$: scattering coefficient

3.2. Radar equation for bedrock surface

The radar equation for the bedrock surface can be derived similarly except for the rising part as shown in Fig. 3(a) section (III). The reason why the rising part can't be used is that the full energy of the pulse is not yet present. Referring to the Fig. 3(d), the received power from the bedrock/ice interface when the inner ice layer is assumed to be a uniform medium (see Appendix I) is given as follows:

$$P_r=\frac{P_tG^2\lambda^2he^{-2\kappa z/\cos\alpha}\Gamma^2\sigma_R^0(\alpha)f^2(\theta)\cos^3\theta}{2^6\pi^2H^3L^2\left(1+\dfrac{z}{nH\xi}\right)\left(1+\dfrac{z}{nH\xi^3}\right)^2\xi^2} \tag{2}$$

here, Γ and σ_R^0 are transmission and scattering coefficients at the boundary between air and ice, κ is attenuation coefficient, n is the refractive index, z is the ice thickness which can be calculated from the time difference between two peaks, α is the refractive angle (equal to the incidence angle to the bedrock) and is related to θ through Snell's

law, and ξ is defined as

$$\xi=\frac{\cos\alpha}{\cos\theta}\ .$$

In addition, θ can be calculated from the delay time using the following relation:

$$\frac{H}{\cos\theta}+\frac{nz}{\cos\alpha}=\frac{c\tau}{2}\ .$$

3.3. Radar equation for inner region of the ice sheet

The received power P_r from the inner region of the ice sheet is calculated in eq. (3). Echoes from the inner region of the ice sheet which have the same propagation path length from the antenna are received simultaneously, as shown in Fig. 3(c).

$$\begin{cases} P_r=\dfrac{P_t G^2\lambda^2\left(\dfrac{h}{n}\right)\Gamma^2\sigma_v}{2^6\pi^2H^2L^2}\cdot F_1 \\ F_1=\displaystyle\int_0^{\theta_d}\sin\theta'\cos^3\theta'\frac{f^2(\theta')e^{-2\kappa z'/\cos\theta'}}{\left(1+\dfrac{z'}{nH\xi}\right)\left(1+\dfrac{z'}{nH\xi^3}\right)\xi}d\theta' \end{cases} \tag{3}$$

Here θ_d is the incident angle of the crossed point between surface and reflection volume as shown in Fig. 3(c). Details are given in Appendix II. In addition, we use the volumetric scattering coefficient, σ_v, as discussed in section 1, is independent of incidence angle. In the case of a narrow beam, eq. (3) may be approximated by;

$$\begin{cases} P_r=\dfrac{P_t G^2\lambda^2\left(\dfrac{h}{n}\right)\Gamma^2\sigma_v}{2^6\pi^2H^2L^2}F_0 \\ F_0=\dfrac{\theta_0^2e^{-2\kappa z}}{\ln 2\left(1+\dfrac{z}{nH}\right)^2} \end{cases} \tag{4}$$

The antenna pattern is approximated as a Gaussian function which fits the measured pattern well.

$$f(\theta)=\exp\left[-\frac{\theta^2}{(\theta_0/2)^2}\ln 2\right]$$

θ_0 is the beam width at half maximum.

Figure 4 compares results from eqs. (3) and (4) using the actual radar parameter given in Table 1. It shows an example of the difference between F_0 and F_1 in these equations, with altitude $H=300$ m, and attenuation coefficient $\kappa=0$. Though, in this case, the difference of two estimations is smaller than 1.5 dB, the difference will become larger as the attenuation coefficient increases. As eq. (4) has simple form, we used

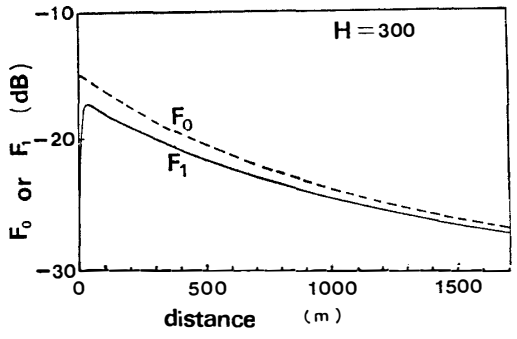

Fig. 4. An example of the difference between F_0 and F_1, where $H=300$ m.

this equation to obtain preliminary results for σ_v and κ but we used eq. (3) in the final analysis. Final results were found using the preliminary value in a least square solution of eq. (3).

4. Radio Scattering Characteristics of Ice

Our analysis begins by determining the attenuation coefficient, κ, and volume scattering coefficient, σ_v, of inner ice from the regression of data from region (II). Then, from data of regions (I) and (III), we can calculate the dependence on incidence angle of the surface scattering coefficients of the ice sheet and the bedrock by applying eqs. (1) and (2), respectively. In these processes, we use the simultaneously recorded navigation data. The attenuation coefficient α_e and scattering coefficient $\Gamma^2\sigma_v$ which

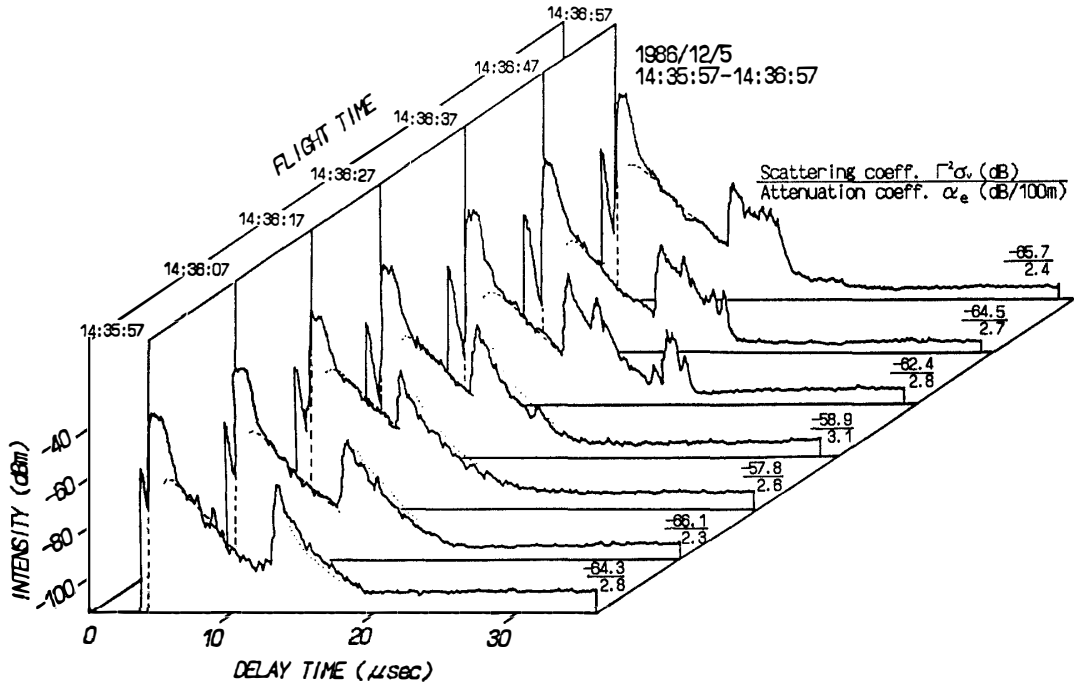

Fig. 5. Results of inferred attenuation coefficient and scattering coefficient. Dashed curves are calculated A-scope curves using radar equations (3) and dotted curves are calculated using equation (2). The volumetric scattering and attenuation coefficients of the ice are shown beside each A-scope trace.

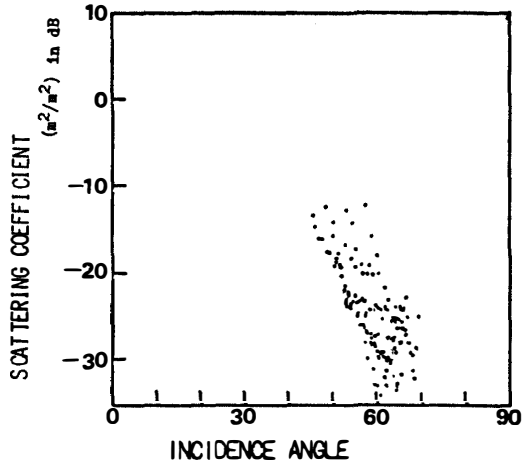

Fig. 6. Surface scattering coefficients of ice sheet surface σ_S^0 as functions of incidence angles derived from equation (1).

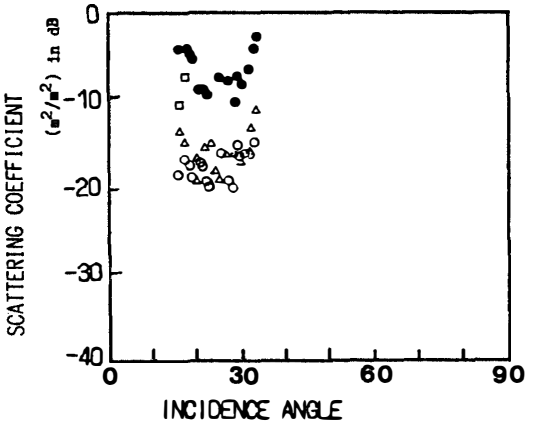

Fig. 7. Surface scattering coefficients of bedrock $\Gamma^2\sigma_R^0$ as a function of incidence angles derived from equation (2). Each symbol shows different A-scope data. ○ is inferred from the data at 1435:57, □ is from the data at 1436:07, ● is from the data at 1436:18 and △ is from the data at 1436:28.

are inferred from this analysis are shown in Fig. 5, where the attenuation coefficient is defined as $\alpha_e=434.3\times\kappa$ (dB/100 m) and the scattering coefficient is defined as $\Gamma^2\sigma_v$ for convenience because it appears in a body in eq. (3). Figure 5 shows seven A-scope traces selected to analyze from Fig. 1. The analyzed data were originally observed on the Antarctic ice sheet about 40 km west of Asuka Camp. Dashed curves show results of regression by using equation (3) and inferred parameters. Good agreement can be found in region (II) between the raw data and the results of regression.

The surface scattering coefficients of the ice sheet σ_s^0 were derived from eq. (1) and are shown in Fig. 6. The range of incidence angle ranges was restricted to section (I). It is reasonable that the scattering coefficient shows a decrease within-cidence angle. In this case, however, the dependence is strong.

The surface scattering coefficient results of the bedrock, $\Gamma^2\sigma_R^0$, from eq. (2) are shown in Fig. 7. The range of incidence angle is restricted by the sensitivity of the receiver. No clear dependence of scattering coefficient and incidence angle is indicated. Consequently, the dotted curves in Fig. 5 which show the calculated dependence of the A-scope form by using eq. (2) were determined with constant scattering coefficient, $\Gamma^2\sigma_R^0$.

5. Discussion

Scattering coefficients of ice sheet surface and bedrock were determined from the characteristics of the A-scope form by using expanded radar equations. The dependence of scattering coefficients on the incident angle is related with the roughness of these surfaces (*e.g.*, ULABY *et al.*, 1982). In this case, a very strong dependence between surface scattering coefficient and incidence angle was found, which indicates that the surface was smooth. On the other hand, the weak dependence of bedrock scat-

tering coefficients on incidence angles suggests a very rough bedrock surface. The range of incidence angle was not sufficient, however, to characterize these roughness of boundaries directly. It may be interesting to survey a region with varying roughness character, for example a coastal region including a "marine ice sheet", ice shelf, near mountains, and so on, to map the scattering behavior with actual roughness.

In addition, the attenuation coefficients and volumetric scattering coefficients were also determined by using expanded radar equations. The attenuation coefficients are the important parameters for inferring the ice sheet temperature. The attenuation of radio waves is caused by absorption and scattering. Absorption is related to the imaginary part of permittivity which is a function of temperature.

Acknowledgments

We would like to express our sincere gratitude to Prof. Yasuhiko NAITO who was the wintering leader of the 27th Japanese Antarctic Research Expedition (JARE-27). We are also grateful to all members of the JARE-27 team for logistic and technical support of these observations. In addition, we express many thanks to Dr. R. K. HAWKINS of the Canada Center for Remote Sensing for his stimulating discussions and checking English.

References

HARRISON, C. H. (1973): Radio echo sounding of horizontal layers in ice. J. Glaciol., **12**, 383–397.

NEAL, C. S. (1976): Radio-echo power profiling. J. Glaciol., **17**, 527–530.

PAREN, J. G. and ROBIN, G. de Q. (1975): Internal reflections in polar ice sheets. J. Glaciol., **14**, 251–259.

ULABY, F. T., MOORE, R. K. and FUNG, A. K. (1982): Radar Remote Sensing and Surface Scattering and Emission Theory, Microwave Remote Sensing, Active and Passive, vol. II. Reading, Addison-Wesley Publ.

(Received March 3, 1988; Revised manuscript received January 14, 1989)

Appendix I: Radar Equation for Bedrock

At the bedrock surface, the radio intensity from a transmitter antenna is given by

$$\frac{P_t G f(\theta) \Gamma}{4\pi L} \frac{e^{-\kappa l_2}}{\left(l_1+\frac{l_2}{n}\right)\left(l_1\frac{\cos\alpha}{\cos\theta}+\frac{l_2}{n}\frac{\cos\theta}{\cos\alpha}\right)} \tag{A1}$$

where the parameters are defined as in Section 3, and l_1 and l_2 are path length in the air and ice as defined in Fig. 3(d). This modified intensity is determined from radio wave flux estimate in the refractive media. The $e^{-\kappa l_2}$ factor is attenuation in the ice layer, which is assumed to be homogeneous.

As area struck by pulse is given by

$$(l_1 \sin\theta + l_2 \sin\alpha)\frac{h}{2n}\cdot\sin\alpha \tag{A2}$$

the radar equation is given as

$$\frac{P_t G^2 \lambda^2 h e^{-2\kappa z/\cos\alpha} \Gamma^2 \sigma_R^0(\theta) f^2(\theta)}{2^6 \pi^6 L^2 \left(\frac{H}{\cos\theta}+\frac{z}{n\cos\alpha}\right)\left[\frac{H}{\cos\theta}\left(\frac{\cos\alpha}{\cos\theta}\right)+\frac{z}{n\cos\alpha}\left(\frac{\cos\theta}{\cos\alpha}\right)\right]^2}. \tag{A3}$$

For convenience in calculation, we define the parameter ξ as:

$$\xi=\frac{\cos\alpha}{\cos\theta} \tag{A4}$$

Finally, we obtain objective radar equation.

$$P_r=\frac{P_t G^2 \lambda^2 h e^{-2\kappa z/\cos\alpha} \Gamma^2 \sigma_R^0(\theta) f(\theta) \cos^3\theta}{2^6 \pi^6 H^3 L^2 \left(1+\frac{z}{nH\xi}\right)\left(1+\frac{z}{nH\xi^3}\right)^2 \xi^2} \tag{A5}$$

Appendix II: Radar Equation for Inner Ice Sheet

Received power from the inner ice sheet P_r is given by summing over the whole scattering volume with the same delay time, τ, as shown in Fig. 3(c). The contribution from the incidence angle between θ' and $\theta'+d\theta'$, dP_r is given by using a similar argument as in case of bedrock, and results in the following:

$$dP_r=\frac{P_t G^2 f^2(\theta') \lambda^2 e^{-2\kappa l_2} \sigma_v}{(4\pi)^3 \left(l_1+\frac{l_2}{n}\right)\left(l_1\frac{\cos\alpha'}{\cos\theta'}+\frac{l_2}{n}\frac{\cos\theta'}{\cos\alpha'}\right)^2} \sin\theta'\left(l_1\frac{\cos\alpha'}{\cos\theta'}+\frac{l_2}{n}\frac{\cos\theta'}{\cos\alpha'}\right)\frac{h}{2n}2\pi d\theta' \tag{A6}$$

therefore P_r is given by integration of eq. (A6) with the condition of constant time delay, τ. τ, θ' and z' are related by eq. (A7), and are related by Snell's law.

$$\frac{H}{\cos\theta'}+\frac{nz'}{\cos\alpha'}=\frac{c\tau}{2} \tag{A7}$$

As eq. (A6) cannot be integrated analytically, the integration F_1 is given numerically.

$$F_1=\int_0^{\theta_d} \sin\theta' \cos^3\theta' \frac{f^2(\theta') e^{-2\kappa z'/\cos\theta'}}{\left(1+\frac{z'}{nH\xi}\right)\left(1+\frac{z'}{nH\xi^3}\right)\xi} d\theta' \tag{A8}$$